Tomographic reconstruction of combustion flow fields from density measurements based on physics-informed neural networks

Johannes Gürtler[1,*], Sami Tasmany[2], Jakob Woisetschläger[2], Robert Kuschmierz[1], Jürgen Czarske[1]

1: Laboratory of Measurement and Sensor System Technique, Technische Universität Dresden, Germany
2: Institute for Thermal Turbomachinery and Machine Dynamics, Graz University of Technology, Austria
*Corresponding author: johannes.guertler@tu-dresden.de

Keywords: Tomography, Physics-Informed Neural Networks, Holography, Combustion, High-Speed Imaging.

ABSTRACT

Achieving stable, low-emission combustion with green hydrogen is crucial for climate-neutral ground-based power generation in turbomachinery. Lean combustion modes with green hydrogen reduce fuel consumption but increase unsteadiness. Thus, multimodal detection techniques for parameters like density and flow velocity are essential to understand the interconnected behavior of combustion, advection velocity and noise production. We previously introduced a high-speed camera-based laser interferometric vibrometer system to detect thermoacoustic oscillations and record advection velocities, using interferometric detection of density fluctuations and correlation-based velocity estimation. However, this method only estimates integral velocity fields, necessitating the solution of the inverse problem. This is relying on iterative optimization, which is computationally expensive and struggles with high dimensional, noisy or limited data. Physics-Informed Neural Networks offer an innovative and efficient approach to these problems, combining neural network flexibility with physical law constraints to unravel intricate cause-effect relationships. Here an approach for reconstructing local velocity fields from a single projection velocity calculated from integral density data is presented. Using a U-net and model assumptions for coupling local and integral velocity fields, the training minimizes errors between measured integral input fields and the predicted local field integrals. The comparison of measured local velocity and the network prediction achieved a relative mean squared error of 3 %.

1. Introduction

Ensuring reliably stable, low-emission combustion with green hydrogen represents a crucial contemporary advancement for attaining climate-neutral ground-based power generation within the field of turbomachinery (“Energy Systems”, 2023). Lean combustion modes associated with green hydrogen enable a reduced fuel consumption, yet exhibit increased unsteadiness, leading to amplified noise and instability attributable to thermoacoustic oscillations. Hence, it becomes essential to employ multimodal detection techniques, particularly for parameters like density and flow

velocity. This approach is necessary to comprehend the interconnected behavior of combustion, advection velocity, noise production, and noise dampening, critical for ensuring stable combustion and advancing environmental protection.

The measurement of density oscillations entails the detection of the refractive index of gases, which is directly related to density through the Gladstone-Dale constant, contingent upon the molecular properties of the gas. Traditionally, refractive index measurements involve holographic or interferometric methods, facilitated by sophisticated high-speed cameras. These techniques have found practical applications in combustion research, including the assessment of fluctuations in flame temperature and heat release rate (Rastogi, 2019; Leitgeb, 2013).

Previously we introduced a high-speed camera-based laser interferometric vibrometer (CLIV) system that enabled the detection of thermoacoustic oscillations and seedingless recording of advection velocities (Greiffenhagen et al., 2020; Gürtler et al., 2021). The measurement approach relied on interferometric detection of density fluctuations within a turbulent and reactive fluid flow. Subsequently, the flow velocity was computed based on the movement of detected density structures, which were determined using image correlation techniques, resulting in a low average uncertainty of $0.6 \cdot 10^{-2}\ \mathrm{m/s}$. However, this approach allows only for the estimation of integral velocity fields and, thus, the solution of the inverse problem is required.

Such inverse problems involve deducing the causes or parameters of a system from observed outcomes, which is inherently challenging due to the ill-posed nature of the problem. Traditional methods for solving inverse problems often rely on iterative optimization techniques, which are computationally expensive and struggle with high-dimensional and especially noisy data. The advent of Physics-Informed Neural Networks (PINNs) has introduced a transformative paradigm, offering an innovative and efficient approach to tackle the complexities associated with inverse problems (Wang et al., 2020). By combining the flexibility of neural networks with the inherent constraints of physical laws, PINNs have emerged as powerful tools for unraveling intricate relationships between cause and effect in the field of flow metrology (Molnar et al., 2023; Mao et al., 2020), enabling accurate and rapid solutions to previously intractable inverse problems.

In this paper we present a physics-informed neural network based approach for those reconstructions, allowing the estimation of local velocity fields from a single projection velocity calculated from integral density data. The approach is based on the combination of a U-net and a model assumption for the coupling of local and integral velocity fields. Training is performed by minimizing the error between the measured integral input field and the integral of the unknown and predicted local field. It is shown, that the chosen physical constrains lead to a meaningful reconstruction result with a relative deviation of $3\ \%$.

2. Approach

Setup The used burner consists of two housing parts, a movable spigot and an inner swirl body that separates the outer and inner chambers. The fuel used is propane gas ($\mathrm{C_3H_8}$), which, like the air, is fed into the outer chamber of the burner via four connections on the upper part of the housing. The connections are radially symmetrical on the side of the housing and feed propane and air alternately into the burner. The swirl is created by four tangential holes in the swirl body, through which the air-propane mixture flows into the inner chamber of the burner. Finally, the swirled flow exits the inner chamber through the burner nozzle with the opening radius $7.5\ \mathrm{mm}$. The geometry of the burner nozzle can be adjusted by the axial position of the spigot and thus allows the outlet velocity and therefore the swirl rate to be varied. The air mass flow rate is adjusted to $0.5\ \mathrm{g/s}$ using a controller of the type *8626* from the manufacturer *Bürkert*, while the mass flow rate of the propane gas is adjusted to $0.039\ \mathrm{g/s}$ using a controller of the type *red-y smart series* from the manufacturer *Vögtlin Instruments GmbH*. This results in a swirl number of 0.47 and thus an applied flame with a comparably small recirculation zone.

The used full-field CLIV system is a holographic interferometer, based on an on-axis heterodyne Mach-Zehnder setup using a narrowband $532\ \mathrm{nm}$ laser (Cobolt Samba) as light source. The laser is split up into a reference path, guided through a cascade of two acousto-optical modulators generating the carrier frequency f_B and a measurement path, where the collimated laser beam is magnified to a diameter of $80\ \mathrm{mm}$, before being imaged onto the high-speed camera (Phantom v1610) using a telecentric lens setup offering a spatial resolution of $140\ \mu\mathrm{m}^2$ per pixel. The camera operated at a frame rate of $120\ \mathrm{kHz}$ using 384×208 pixel, resulting in a field of view of approximately $53 \times 29\ \mathrm{mm}$. Both beams interfere on the camera sensor and at every pixel the interferometric intensity signal $I(t) \sim I_0 \cos\left(\Delta\varphi(t) + \varphi_0\right)$, with the amplitude I_0, the phase offset φ_0 and the time dependent phase shift

$$\Delta\varphi(t) = 2\pi f_\mathrm{B} t + \frac{2\pi}{\lambda} L(t) \tag{1}$$

is detected, with the laser wavelength λ and the length of the optical path

$$L(t) = \int n(t)\mathrm{d}z \tag{2}$$

along the laser beam in z-direction with the refractive index n, which is linear depending on the fluids density ρ, according to the Gladstone-Dale relation

$$G = \frac{n-1}{\rho} \tag{3}$$

with the material dependent Gladstone-Dale constant G. Combining Eq. (1)-(3) and differentiation exhibits the linear relation between the instantaneous frequency

$$f_I = \frac{\mathrm{d}\Delta\varphi}{2\pi\mathrm{d}t} = f_\mathrm{B} + \frac{\dot{L}}{\lambda} = f_\mathrm{B} + \frac{G}{\lambda}\int \dot{\rho}\mathrm{d}z = f_\mathrm{B} + \frac{G}{\lambda}\dot{\rho}_\mathrm{LOS} \tag{4}$$

of the intensity signal and the temporal density fluctuations $\dot{\rho}_{\mathrm{LOS}}$, detected line of sight (LOS) along the laser beam in z-direction. Please note, that the variance of the Gladstone-Dale constant within the measurement volume is negligible and therefore not dependent on z.

The instantaneous frequency f_I is calculated from the cameras intensity signal by generating the complex analytic signal

$$a[k] = \cos\left(\Delta\varphi[k]\right) + j\sin\left(\Delta\varphi[k]\right) \tag{5}$$

for every sample k, using the FFT-based Hilbert transform and evaluating its instantaneous phase. In order to increase computational speed, phase unwrapping is avoided by differentiation of Eq. (4) before computing the instantaneous phase, by using the complex conjugate a^* of the analytic signal, shifted by one sample:

$$f_I[k] = \frac{1}{2\pi}\mathrm{angle}\left(a^*[k-1]\cdot a[k]\right). \tag{6}$$

The spectral range of detectable density oscillations is limited by the camera's frame rate and the chosen carrier frequency. Here the carrier was adjusted to $f_{\mathrm{B}} = 40\ \mathrm{kHz}$, enabling the detection of density oscillations and higher harmonics within the range of $\pm 20\ \mathrm{kHz}$, considering the detectable frequency range of the intensity signal up to $60\ \mathrm{kHz}$ due to the camera's frame rate.

From the LOS density data, measured with CLIV, the integral advection velocity is calculated using image correlation. The correlation is processed in Matlab with the open source tool PIVlab (Thielicke & Stamhuis, 2014), using 4 iterative correlations with reducing window size ([40, 32, 24, 16] pixel) and $70\ \mathrm{kHz}$ window overlap. In order to increase accuracy, image pre-processing for contrast enhancement (Contrast Limited Adaptive Histogram Equalization, high pass filtering) and a 2D Gaussian subpixel finder as well as spline-based window deformation were used. The integral velocity is then further processed using the physics-informed neural network approach.

Physics-informed neural networks Inverse problems, ubiquitous in various scientific and engineering disciplines, involve deducing the causes or parameters of a system from observed outcomes. These problems are inherently challenging due to their ill-posed nature, where multiple configurations can lead to the same observations. Traditional methods for solving inverse problems often rely on iterative optimization techniques, which can be computationally expensive and struggle with high-dimensional and noisy data. The advent of Physics-Informed Neural Networks (PINNs) has introduced a transformative paradigm, offering an efficient approach to tackle the complexities associated with inverse problems. By combining the flexibility of neural networks with the inherent constraints of physical laws, PINNs have emerged as powerful tools for unraveling intricate relationships between cause and effect, enabling accurate and rapid solutions to previously intractable inverse problems (Mao et al., 2020). PINNs leverage the expressive power

of neural networks to learn complex patterns from data, while also enforcing physical consistency through the incorporation of governing equations and constraints. This physics-informed approach significantly enhances the robustness of inverse problem solutions, even when dealing with noisy data.

Here such a network is used for the tomographic reconstruction of the integral advection velocity, which was calculated as described above. Based on the assumption, that the correlation of the integral density time signal is weighted by the power of the density change along the laser beam, we assume that the detected velocity can be described by the following model:

$$v_{\mathrm{recon}}(x,y) = \int \frac{v(x,y,z)P(x,y,z)}{P_{\mathrm{LOS}}(x,y)}\mathrm{d}z, \tag{7}$$

where P is the power of the detected density change and the index LOS marks the line-of-sight integral data. The local power signal is calculated from the LOS power using the inverse Abel transform under the assumption of rotational symmetry, which is valid for time averaged data of the flame used. The network principle is depicted in Fig. 1. The integral velocity field v_{in} is calculated by correlation of integral density data, measured in the swirl-stabilized flame. From this single input the dense U-net predicts the local in-plane velocity v_{out} which is then used for reconstruction of the integral velocity field v_{recon} based on the above model assumption. Training of the network is performed iteratively using the mean squared error between v_{in} and v_{recon} and the gradient of v_{out} as loss function $m = \frac{1}{N}(||v_{\mathrm{in}} - v_{\mathrm{recon}}||_2^2 + ||\nabla v_{\mathrm{out}}||_2^2)$.

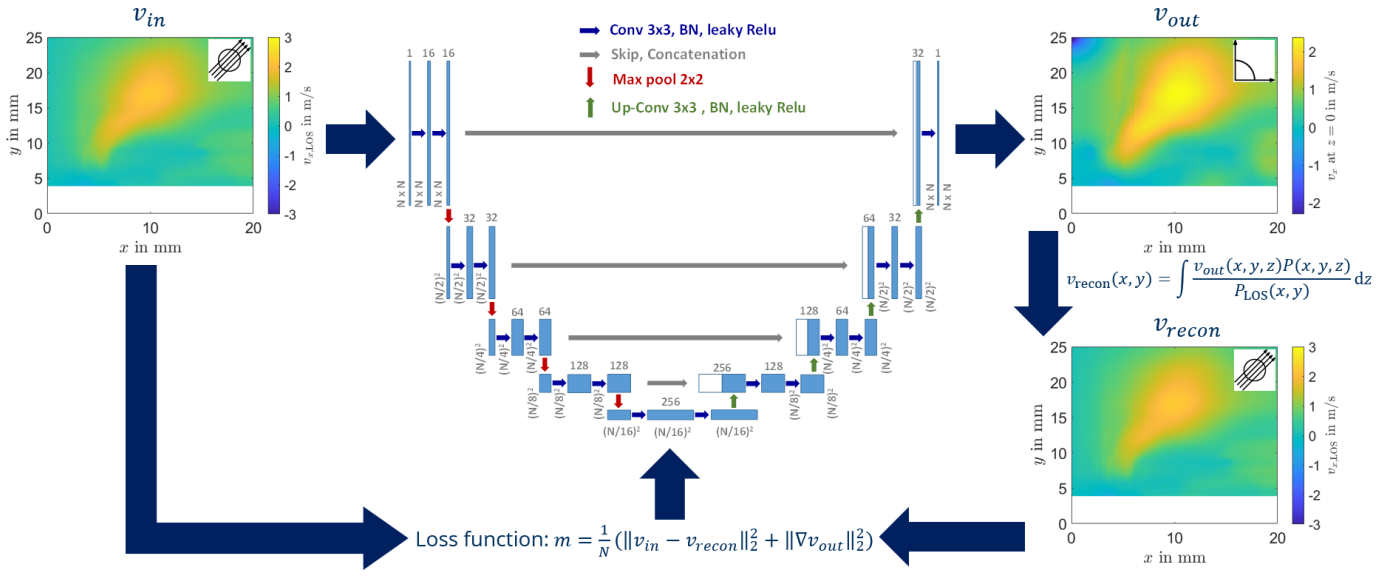

Figure 1. Physics-informed neural network approach for tomographic reconstruction of local in-plane velocity fields. The integral velocity field v_{in} is fed into the dense U-net, which predicts the local velocity v_{out}. This is used for calculating the integral velocity field v_{recon} based on the given model assumption. Training of the network is performed iteratively using the given loss function.

3. Results and Discussion

The network performance for reconstructing a single velocity component v_x in x-direction is depicted in Fig. 2, where (a) shows the integral input data, (b) the output of the U-Net, i. e. the local in-plane velocity at $z = 0$ mm, (c) the network loss and (d) the deviation between input and the reconstruction of the output using Eq. (7). As a result, the network loss converges after 600 s, running on a single GPU *NVIDIA RTX 3090*. The highest deviation is detectable near the rotation axis of the flame at $x = 0$ mm, which is typical for tomographic reconstruction. Furthermore, it is visible, that the deviation increases in regions with higher velocity values. The mean deviation averaged over the full image amounts to 0.195 m/s, i. e. 4 % of the maximum velocity.

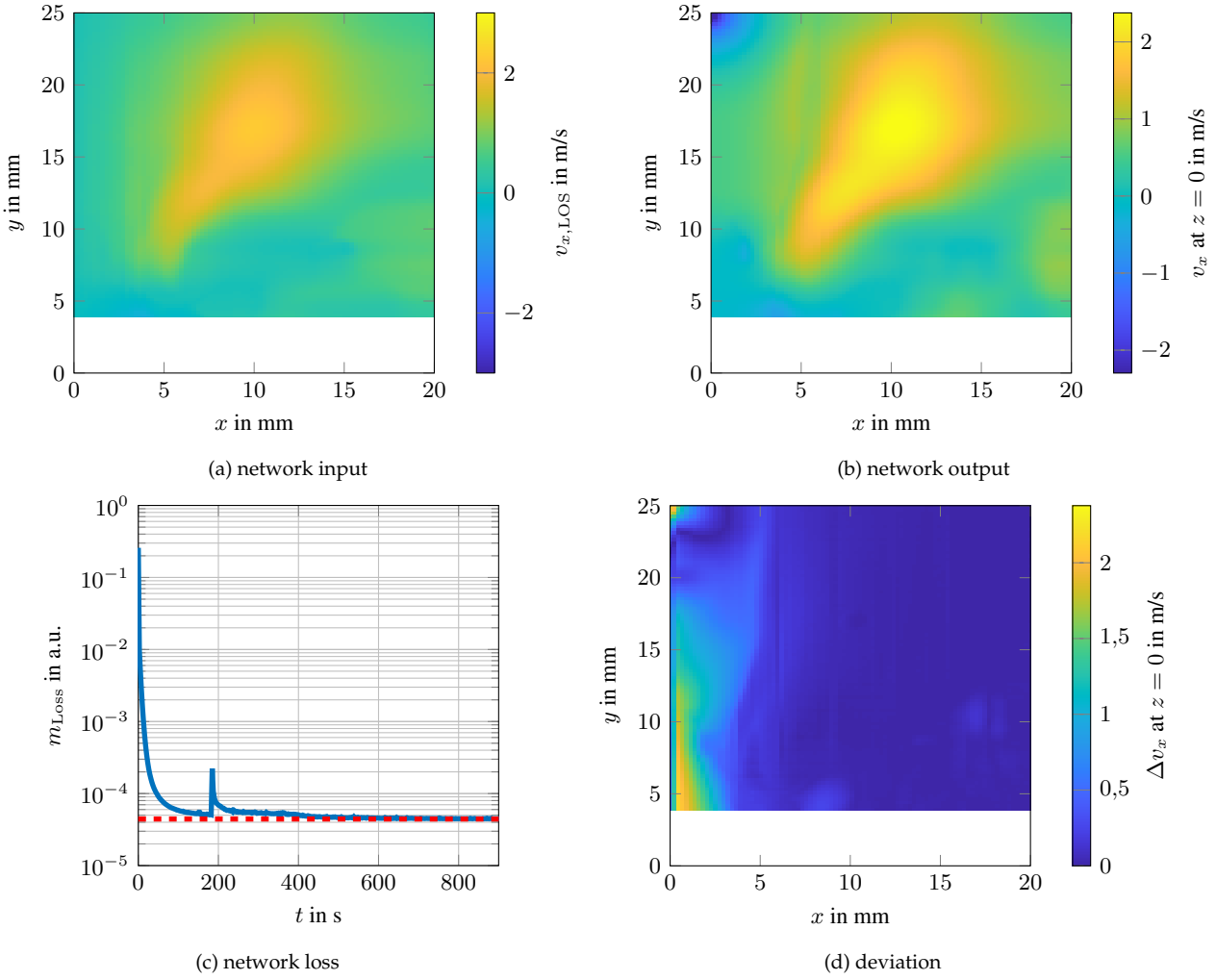

Figure 2. Network performance for a single velocity component v_x in x-direction. (a) shows the integral input data, (b) the output of the U-Net, i. e. the local in-plane velocity at $z = 0$, (c) the network loss and (d) the deviation between input and the reconstruction of the output using Eq. (7).

For further evaluation of the network capabilities, data of the local flow velocity measured by Doppler global velocimetry with frequency modulation was used as a reference (Schlüßler et al.,

2015). The local velocity was transformed into integral velocity data using Eq. (7) and fed into the network. The result for the absolute value of the two-component in-plane velocity at $z = 0$ mm is shown in Fig. 3, where (a) is the directly measured local velocity using particle-based Doppler global velocimetry, (b) the predicted local velocity field using the physics-informed neural network approach and (c) the deviation between measurement and prediction. The network prediction achieved a mean squared error of 0.185 m/s, while flow velocities up to 6 m/s where detected. Additionally the structural similarity index between the measured and predicted flow field calculates to 91 %.

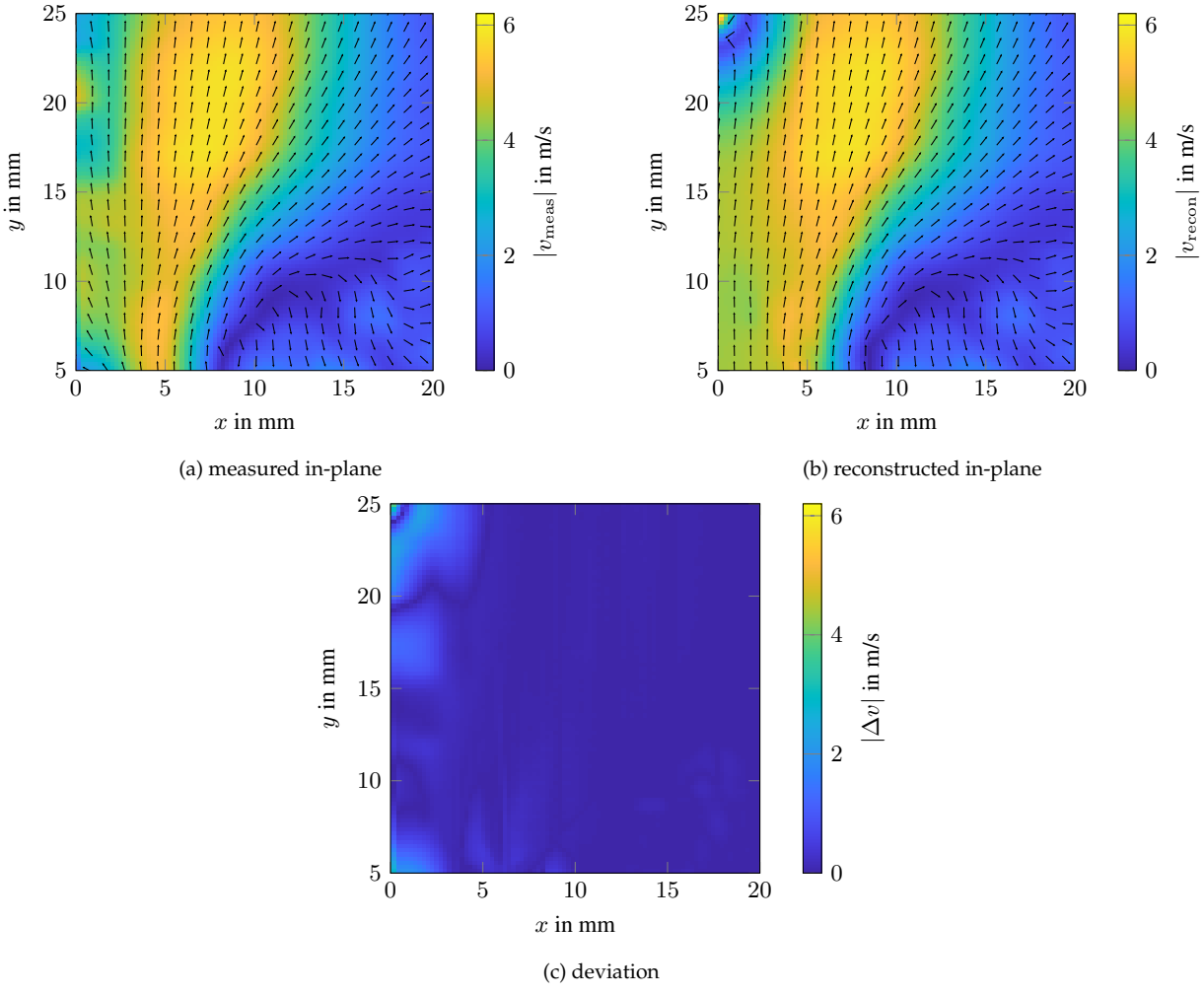

Figure 3. Comparison of the absolute value of the two-component in-plane velocity at $z = 0$ mm. (a) Directly measured local velocity using particle-based Doppler global velocimetry. (b) Predicted local velocity field using the physics-informed neural network approach. (c) Deviation between measurement and prediction.

While the results show a good agreement between measurement and network output, this gives no validation of the model assumption Eq. (7), since the network input was calculated by this model. However, the meaningful results prove that the chosen physical constraints used for calculation of the network loss are in principle capable for usage in such tomographic reconstruction of flow

fields. Further improvements are possible by increasing the number of projection angles, enabling the reconstruction of all three velocity components. Overall, the PINN-based approach proves to be a valuable new tool for flow metrology.

4. Conclusion

In conclusion, achieving stable, low-emission combustion with green hydrogen is vital for climate-neutral ground-based power generation in turbomachinery. Lean combustion modes introduce challenges such as increased unsteadiness and thermoacoustic oscillations. Multimodal detection techniques, particularly for density and flow velocity, are essential to understand and mitigate these issues. Traditional methods like holographic and interferometric techniques using high-speed cameras have advanced combustion research, enabling the assessment of critical parameters. Our previously introduced high-speed camera-based laser interferometric vibrometer system successfully detected thermoacoustic oscillations and recorded advection velocities without seeding, although it only estimated integral velocity fields.

The challenge of solving inverse problems, due to their ill-posed nature and computational complexity, has been effectively addressed by Physics-Informed Neural Networks (PINNs). These networks combine neural network flexibility with physical law constraints, offering accurate and efficient solutions. Our PINN-based approach reconstructs local velocity fields from integral density data, demonstrating high accuracy with a mean squared error of 0.185 m/s and detecting flow velocities up to 6 m/s. The results prove that the physical constrains chosen here allow meaningful tomographic reconstructions. Improvements are possible by using multi-angle detection in order to reconstruct all three velocity components. Furthermore, physical models such as Navier-Stokes equations should improve and generalize the network applicability.

Acknowledgements

This research is the result of Austrian-German joint research project, funded by the Austrian Science Fund FWF within Grant No. FWF-I5392-N and project DFG CZ 55/50-1 funded by the German Research Foundation DFG. This project is a Lead-Agency D-A-CH project in cooperation between Graz University of Technology, Austria and Technische Universität Dresden, Germany.

References

Energy Systems. (2023). In Intergovernmental Panel on Climate Change (IPCC) (Ed.), *Climate Change 2022 - Mitigation of Climate Change: Working Group III Contribution to the Sixth Assessment*

Report of the Intergovernmental Panel on Climate Change (pp. 613–746). Cambridge: Cambridge University Press. doi: 10.1017/9781009157926.008

Greiffenhagen, F., Woisetschläger, J., Gürtler, J., & Czarske, J. (2020, January). Quantitative measurement of density fluctuations with a full-field laser interferometric vibrometer. *Experiments in Fluids*, *61*(1), 9. doi: 10.1007/s00348-019-2842-y

Gürtler, J., Greiffenhagen, F., Woisetschläger, J., Kuschmierz, R., & Czarske, J. (2021, April). Seedingless measurement of density fluctuations and flow velocity using high-speed holographic interferometry in a swirl-stabilized flame. *Optics and Lasers in Engineering*, *139*, 106481. doi: 10.1016/j.optlaseng.2020.106481

Leitgeb, T. (2013). Interferometric determination of heat release rate in a pulsated flame. *Combustion and Flame*. doi: 10.1016/j.combustflame.2012.11.001

Mao, Z., Jagtap, A. D., & Karniadakis, G. E. (2020, March). Physics-informed neural networks for high-speed flows. *Computer Methods in Applied Mechanics and Engineering*, *360*, 112789. doi: 10.1016/j.cma.2019.112789

Molnar, J. P., Venkatakrishnan, L., Schmidt, B. E., Sipkens, T. A., & Grauer, S. J. (2023, January). Estimating density, velocity, and pressure fields in supersonic flows using physics-informed BOS. *Experiments in Fluids*, *64*(1), 14. doi: 10.1007/s00348-022-03554-y

Rastogi, V. (2019). Holographic optical element based digital holographic interferometer for the study of macro flames, micro flames and their temperature instability. *Optics and Lasers in Engineering*. doi: 10.1016/j.optlaseng.2019.05.021

Schlüßler, R., Bermuske, M., Czarske, J., & Fischer, A. (2015, October). Simultaneous three-component velocity measurements in a swirl-stabilized flame. *Experiments in Fluids*, *56*(10), 183. doi: 10.1007/s00348-015-2055-y

Thielicke, W., & Stamhuis, E. J. (2014, October). PIVlab – Towards User-friendly, Affordable and Accurate Digital Particle Image Velocimetry in MATLAB. *Journal of Open Research Software*, *2*. doi: 10.5334/jors.bl

Wang, F., Bian, Y., Wang, H., Lyu, M., Pedrini, G., Osten, W., … Situ, G. (2020, May). Phase imaging with an untrained neural network. *Light: Science & Applications*, *9*(1), 77. doi: 10.1038/s41377-020-0302-3